JOURNAL OF BACTERIOLOGY, May 2007, p. 3573–3580 Vol. 189, No. 9
0021-9193/07/$08.00+0 doi:10.1128/JB.01083-06

Crystal Structure of Uroporphyrinogen Decarboxylase from *Bacillus subtilis*▽

Jun Fan,[1,2] Qun Liu,[3] Quan Hao,[3] Maikun Teng,[1,2]* and Liwen Niu[1,2]*

Hefei National Laboratory of Physical Sciences at Microscale and School of Life Sciences, University of Science & Technology of China, Hefei Anhui, 230027, China[1]; Key Laboratory of Structural Biology, Chinese Academy of Sciences, Hefei, Anhui, 230037, China[2]; and MacCHESS, Cornell High Energy Synchrotron Source, Cornell University, Ithaca, New York 14853[3]

Received 2 August 2006/Accepted 12 November 2006

Uroporphyrinogen decarboxylase (UROD) is a branch point enzyme in the biosynthesis of the tetrapyrroles. It catalyzes the decarboxylation of four acetate groups of uroporphyrinogen III to yield coproporphyrinogen III, leading to heme and chlorophyll biosynthesis. UROD is a special type of nonoxidative decarboxylase, since no cofactor is essential for catalysis. In this work, the first crystal structure of a bacterial UROD, *Bacillus subtilis* UROD ($UROD_{Bs}$), has been determined at a 2.3 Å resolution. The biological unit of $UROD_{Bs}$ was determined by dynamic light scattering measurements to be a homodimer in solution. There are four molecules in the crystallographic asymmetric unit, corresponding to two homodimers. Structural comparison of $UROD_{Bs}$ with eukaryotic URODs reveals a variation of two loops, which possibly affect the binding of substrates and release of products. Structural comparison with the human UROD-coproporphyrinogen III complex discloses a similar active cleft, with five invariant polar residues (Arg29, Arg33, Asp78, Tyr154, and His322) and three invariant hydrophobic residues (Ile79, Phe144, and Phe207), in $UROD_{Bs}$. Among them, Asp78 may interact with the pyrrole NH groups of the substrate, and Arg29 is a candidate for positioning the acetate groups of the substrate. Both residues may also play catalytic roles.

Tetrapyrroles, including heme, chlorophyll, siroheme, and vitamin B_{12}, are a family of structurally related cofactors and prosthetic groups with different central metal ion insertions. The common pathways in tetrapyrrole biosynthesis start from the first precursor 5-aminolevulinate. Two molecules of this compound are condensed to generate porphobilinogen (PBG). Four molecules of PBG are further condensed by PBG deaminase (PBGD) to generate hydroxymethylbilane, which is subsequently cyclized to generate either uroporphyrinogen III (urogen III), by urogen III synthase with inversion of the D pyrrole ring, or isomer urogen I, by nonenzyme catalysis. urogen III is the last common precursor of all tetrapyrroles in living cells, at which major branching of the biosynthetic pathways happens. Bismethylation of urogen III by urogen methyltransferase (UPMT) generates procorrin-2, an intermediate in the biosynthesis of siroheme and vitamin B_{12}. Alternatively, decarboxylation of urogen III at C-2, C-7, C-12, and C-18 by urogen decarboxylase (UROD; EC 4.1.1.37) forms coproporphyrinogen III (coprogen III). This compound can then be converted to proporphyrinogen IX by coprogen III oxidase (CPOX), leading to the biosynthesis of heme and chlorophyll (8). The pathways of polymerization of PBG by PBGD and modification of porphyrinogen's side chains by the enzymes UROD, UPMT, and CPOX are shown in Fig. 1.

UROD is the first nonoxidative decarboxylase that is independent of cofactors or prosthetic groups (6, 32). The pyrrole rings of urogen III are thought to function as an electron sink that promotes electron withdrawal in a way similar to that of the pyridine ring of pyridoxyl phosphate (2). Biochemical assays demonstrate the existence of one or more active sites in the enzyme (2, 6). Under physiological conditions, the sequential decarboxylation initiates at the acetate side chain of the pyrrole ring D, followed by rings A, B, and C. However, with surplus substrates, decarboxylation tends to happen in a random order (20). UROD has a relatively broad substrate specificity, including urogen III, its isomer urogen I, and their partially decarboxylated intermediates. The selective inhibition of one or more decarboxylation steps by heating, porphyrinogens, or porphyrins has been observed for URODs from different sources (7). A deficiency of UROD has been found in patients with sporadic porphyria cutanea tarda and hepatoerythropoietic porphyria (7). In *Escherichia coli* and *Salmonella enterica* serovar Typhimurium, the natural mutations of URODs cause the cellular accumulation of the oxidative substrate uroporphyrin III and the retardation of colony growth (30, 37).

The crystal structures of human UROD (hUROD) and tobacco UROD (tUROD) reveal that the enzyme is a homodimer, each monomer comprising a single domain containing an α/β-barrel with a deep active-site cleft (21, 35). Based on the structures of the hUROD-product complex, Arg37 and Arg41 have been proposed to interact with propionate groups of products, and Asp86 has been thought to interact with pyrrole NH groups and likely promotes the catalysis by stabilizing a positive charge on a reaction intermediate (28).

Compared with eukaryotic URODs, bacterial UROD is less understood, with only one report which describes the charac-

* Corresponding author. Mailing address: Hefei National laboratory of Physical Sciences at Microscale and School of Life Sciences, University of Science & Technology of China, Hefei Anhui, 230027, China. Phone and fax for Maikun Teng: 86-551-3606314. E-mail: mkteng@ustc.edu.cn. Phone and fax for Liwen Niu: 86-551-3603046. E-mail: lwniu@ustc.edu.cn.

▽ Published ahead of print on 22 November 2006.

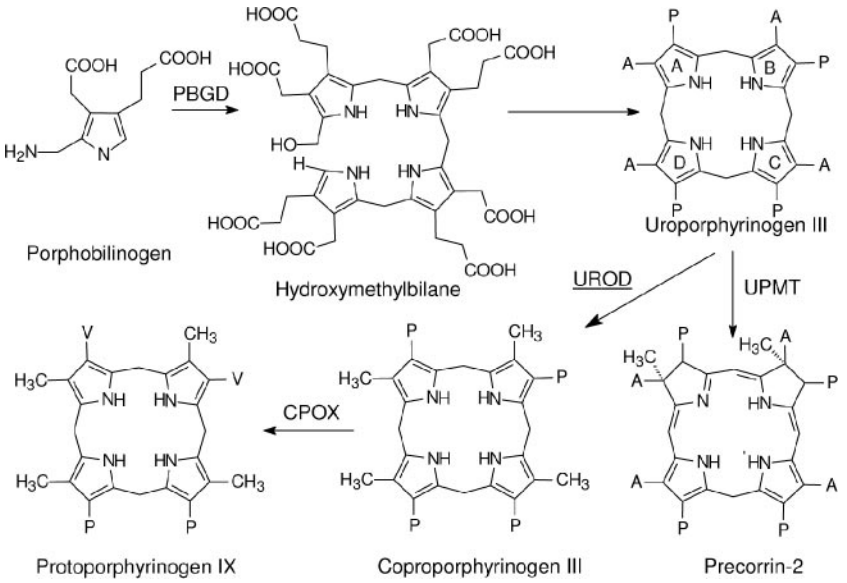

FIG. 1. Pathway for polymerization of PBG and modification of porphyrinogen's side chain in the biosynthesis of tetrapyrroles. The acetate, propionate, and vinyl groups are denoted A, P, and V, respectively. Without the inversion of the D-ring, hydroxymethylbilane cyclizes to form symmetric urogen I. The enzymes responsible for the polymerization of PBG and modification of porphyrinogen's side chains, PBGD, UROD, UPMT, and CPOX, are described in the text. The enzyme UROD, which is the focus of this study, is underlined. The figure was generated using ChemWindow 6.0.

terization of a UROD from *Rhodobacter sphaeroides* (16). In the gram-positive bacterium *Bacillus subtilis*, the genes for enzymes catalyzing the biosynthesis of heme and siroheme are organized in four independent operons (11, 12, 13, 15). UROD is encoded by the *hemE* gene in the *hemEYH* operon (11). Two other genes encode the enzymes responsible for the terminal pathway of heme biosynthesis. These two enzymes have been well studied and display a few special characteristics (8). However, little is known for the *B. subtilis* UROD ($UROD_{Bs}$), a branch-point enzyme that plays a regulatory role in the metabolic flux through the branched pathway of heme biosynthesis. Here, we present the three-dimensional crystal structure of $UROD_{Bs}$ to understand the molecular mechanism of heme biosynthesis in *B. subtilis*.

MATERIALS AND METHODS

Purification, molecular weight determination, and activity assay of $UROD_{Bs}$. The complete *hemE* gene encoding $UROD_{Bs}$ was amplified from *B. subtilis* genomic DNA and cloned into the NdeI/BamHI sites of the expression vector pET-15b (Novagen, United States). The recombinant hexahistidine-tagged $UROD_{Bs}$ was overproduced as a soluble protein in *E. coli* strain BL21(DE3) with isopropyl-β-D-thiogalactopyranoside induction and purified to homogeneity by using a Ni-nitriloacetic acid column (QIAGEN, Germany). The protein samples were concentrated to about 7 mg/ml by ultrafiltration through a YM-10 membrane (Amicon, United States) with 10 mM Tris-HCl buffer, pH 8.0, containing 10 mM β-mercaptoethanol and 200 mM NaCl and were stored at −70°C.

The expression level, enzyme purity, and molecular weight of $UROD_{Bs}$ were determined by sodium dodecyl sulfate-polyacrylamide gel electrophoresis (SDS-PAGE) on 15% polyacrylamide gels. Dynamic light scattering (DLS) measurements were performed at 20°C with a DynaPro-MS800 (Proterion, United States). The molecular weight of $UROD_{Bs}$ was calculated by assuming a globular conformation model, using the software supplied by the manufacturer.

Urogen III was prepared by the reduction of uroporphyrin III with sodium amalgam (16). The enzymatic activity was analyzed spectroscopically at 400 nm ($\varepsilon = 489\ mM^{-1}\ cm^{-1}$), monitoring the concentration of coproporphyrin III extracted with 1 ml ether from the reaction mixture (6). One unit of UROD activity is defined as the amount of enzyme that catalyzes the formation of 1 nM coprogen III in 30 min. Protein concentrations were determined with Coomassie brilliant blue G-250, using bovine serum albumin as the standard.

Crystallization and data collection. The hexahistidine-tagged $UROD_{Bs}$ was crystallized by the hanging-drop method at 20°C. The reservoir solution contained 25% polyethylene glycol-monomethyl ether 2000 and 160 mM sodium acetate in 100 mM citrate, pH 5.6. The hanging-drop solution was made by mixing 1 μl reservoir solution with 2 μl protein solution of 7 mg/ml $UROD_{Bs}$. Crystals as large as 0.4 by 0.3 by 0.1 mm were obtained in 1 week.

The diffraction data were collected from one crystal at BSRF (Beijing, China) under cryogenic protection at 100 K. A total of 320 images were recorded on a MarCCD detector. The raw image data were integrated in the MOSFLM program and merged in the SCALA program after rejecting unreliable diffractions (5). The data collection, reduction, and crystallographic statistics are listed in Table 1.

Structure determination and refinement. The structure of $UROD_{Bs}$ was solved by the molecular replacement method implemented in the AMoRe program (26). The hUROD model (PDB identification number 1URO) was modified before molecular replacement. The amino acid side chains that differed between hUROD and $UROD_{Bs}$ were mutated to glycine residues. Loops with a high B-factor were cropped from the search model. Four clear solutions were obtained from the rotational search using the data between 10 and 3.0 Å, corresponding to four molecules in the crystallographic asymmetric unit of the P_1 cell. In the P_1 space group, the translational vector for the first peak was randomly assigned and fixed during the subsequent translational searching for the other three molecules. The coefficient of correlation increased steadily when more molecules were included for the translational searches. The final coefficient of correlation for the four-molecule model in the asymmetric unit is about 60%.

The model was then subjected to 20 cycles of rigid-body and restraint refinements in the REFMAC program (25). The model phases were improved by density modification with noncrystallographic symmetry averaging before the model building. The averaged density map came from density-modification phases and is a good-quality map for rebuilding the $UROD_{Bs}$ model, including the parts where the structures of hUROD and $UROD_{Bs}$ are different. The strict noncrystallographic-symmetry constraints were used during the iterative model building in the O program and the refinements in the CNS program (4). When the model was completed, the constraints were removed and water molecules were added. Subsequent refinements of $UROD_{Bs}$ by REFMAC resulted in an R factor and R_{free} factor of 19.7% and 25.1%, respectively (see Table 1 footnotes).

Protein structure accession number. The atomic coordinates and diffraction data have been deposited in the Protein Data Bank (http://www.pdb.org/) under the identification number 2INF.

TABLE 1. Crystallographic data collection, reduction, and refinement statistics

Type of measurement	Value
Collection	
Cell dimensions (Å)	a = 58.612, b = 80.410, c = 90.940
Cell dimensions (°)	α = 68.681, β = 89.638, γ = 80.817
Space group	P1
Resolution (Å)	30-2.3 (2.36-2.30)[a]
Wavelength (Å)	1.1
Distance (mm)	140
Mosaicity	0.27
Unique reflections	61,284
Multiplicity	2.4
I/σ	7.3 (1.6)
R_{merge} (%)[b]	6.3 (40.6)
Completeness (%)	96.2
Refinement	
R factor (%)[c]	19.74
R_{free} factor (%)[c]	25.13
No. of protein atoms	10,772
No. of water molecules	256
Ramachandran plot	
Core	94.1%
Allowed	5.6%
Generally allowed	0.3%
Disallowed	0.1%
RMS deviations	
Bond lengths (Å)	0.012
Bond angles (°)	1.290

[a] Values in parentheses are from the highest resolution shell.

[b] $R_{merge} = \Sigma|I - \langle I \rangle|/\Sigma I$, where *I* is the integrated intensity of a given reflection.

[c] $R = \Sigma||Fobs| - |Fcalc||/\Sigma|Fobs|$. R_{free} was calculated using 5% of data excluded from refinement.

RESULTS

Dimerization of the purified $UROD_{Bs}$. DNA sequencing confirms the cloned sequence of *B. subtilis hemE* (11), with the exchange of four bases. Two base changes result in the replacement of Ile156 and Glu198 by Thr156 and Lys198, respectively. Both residues are less conserved in UROD. The base changes are probably attributable to a difference in the *B. subtilis* strain used in this study. The specific activity of $UROD_{Bs}$ is about 560 U/mg protein, suggesting that the 2-amino-acid residue replacement does not cause the loss of activity. The final yield of purified $UROD_{Bs}$ after ultrafiltration is about 10 mg per liter of cell culture.

SDS-PAGE showed that the monomer size of $UROD_{Bs}$ is about 40 kDa (Fig. 2A), corresponding to the analysis of the transcription-translation of *B. subtilis hemE* in vitro (11) and close to the molecular mass (41,797.04 Da) deduced from the sequence of hexahistidine-tagged $UROD_{Bs}$ by the Compute pI/MW tool (http://www.expasy.org). Assuming a globular protein shape, the DLS data were consistent with a homodimer of about 81 kDa (Fig. 2B). The dimerization of $UROD_{Bs}$ in solution is identical with the formation of the dimers of hUROD and tUROD (22, 27).

The overall structure of $UROD_{Bs}$. The structure of the $UROD_{Bs}$ monomer includes amino acid residues 6 to 88 and 101 to 349. The residues 1 to 5, 89 to 100, and 350 to 353 are not visible in the electron density map. The $UROD_{Bs}$ monomer comprises a single domain which consists of a $(\beta/\alpha)_8$ barrel fold. Eight parallel β-strands form a circular β-barrel surrounded by eight α-helices. The core of the $UROD_{Bs}$ barrel, with a diameter of about 15 Å, is built up with four stacked layers containing hydrophobic residues (Fig. 3A). Secondary structure assignments (Fig. 4A) were used as defined in the program ESPript (10), with the exception that residues 24 to 27 were defined as a strand (β1). Strands and helices of the $(\beta/\alpha)_8$ barrel are named β1 to β8 and α1 to α8. All other helices have been given the alphabetical designations αA to αI (Fig. 4A and B). Helices αC, αH, and αI adopt 3_{10} conformations, as do the last three residues of helix α4 and the first three residues of helix α5. The loops between the C-terminal end of each barrel strand and the subsequent barrel helix are numbered L1 to L8 (Fig. 4B). In loop L1, the small loops at both sides of αB are named L1a, including residues 26 to 36, and L1b, including

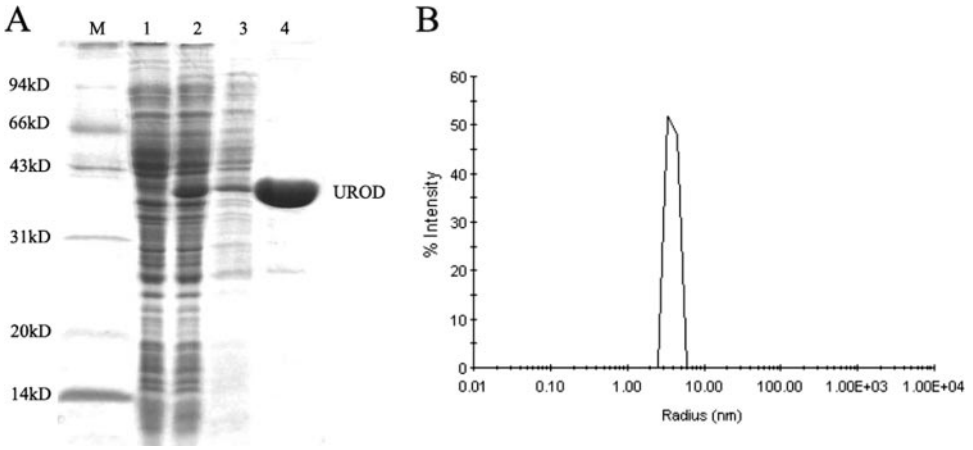

FIG. 2. Determination of molecular mass of $UROD_{Bs}$ by SDS-PAGE (A) and DLS measurements (B). (A) Lanes 1 and 2, total protein from the uninduced and induced cells, respectively; lane 3, soluble protein from the induced cell; lane 4, purified hexahistidine-tagged $UROD_{Bs}$ (20 μg). Protein markers are indicated on the left. (B) The protein samples were dissolved in 10 mM Tris-HCl, 100 mM NaCl, and 10 mM β-mercaptoethanol, pH 7.0, at a concentration of 2 mg/ml.

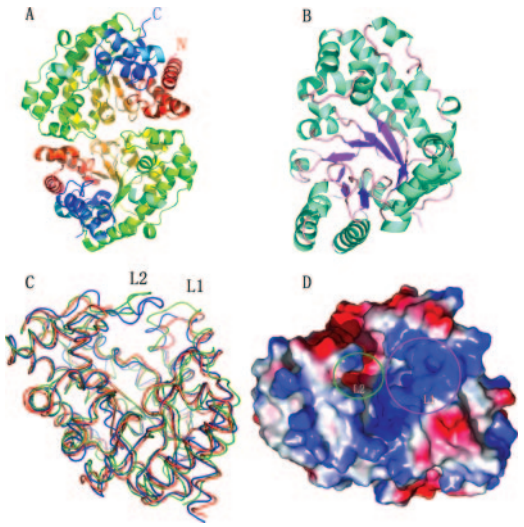

FIG. 3. (A) The $UROD_{Bs}$ dimer in the asymmetric unit. (B) Ribbon diagram of the $UROD_{Bs}$ monomer. (C) Superposition of C_α atoms for the monomer of UROD from *B. subtilis* (red), humans (blue), and tobacco (green), respectively. The L1 and L2 loops are marked. (D) Molecular surface colored (blue, positive; red, negative) according to the electrostatic potentials of the $UROD_{Bs}$ monomer. The areas of the L1 and L2 loops are denoted. The active-site cleft is located in the β-barrel. All colored images in this paper were generated in PYMOL (http://www.pymol.org).

residues 50 to 54. In loop L2, four small loops between the helices are named L2a, including residues 75 to 83; L2b, including residues 87 to 107; L2c, including residues 111 to 118; and L2d, including residues 121 to 123.

Four molecules are observed in the crystallographic asymmetric unit. The root mean square (RMS) deviation in the C_α positions among the various dimers is calculated to be in the range from 0.274 to 0.456 Å. According to the calculation done with CNS, monomer A's solvent-accessible surface area buried at the dimer interface is 2,341 $Å^2$ (Fig. 3B). The dimer formation corresponds with the molecular weight by DLS measurements. The UROD dimer is essential for catalysis, since the Y311C mutant of hUROD retains 60% of the enzyme activity of the wild type, due to some disruption of the dimer interface (24). The crystal structures of hUROD and tUROD reveal one molecule in the asymmetric unit. The dimer in the $UROD_{Bs}$ lattice is analogous to the interasymmetric-unit homodimers of the eukaryotic structures (21, 35). The area buried at the dimer interface of $UROD_{Bs}$ is similar to that of hUROD and tUROD. The dimer interface is remarkably flat and extensive, consisting of a small loop between αF and αG and the five loops L4, L5, L6, L7, and L8.

The amino acid sequence of $UROD_{Bs}$ shows about 36% and 38% identity with tUROD and hUROD, respectively (Fig. 4A). Despite low sequence identity among $UROD_{Bs}$ and two eukaryotic URODs, the overall folding of $UROD_{Bs}$ is similar to that of eukaryotic homologous enzymes (Fig. 3C). The RMS deviation of the C_α positions of 322 structurally equivalent residues of $UROD_{Bs}$ is 1,457 Å for hUROD and 1,500 Å for tUROD. The structural similarity between $UROD_{Bs}$ and hUROD is higher, corresponding to identity of the two enzymes. The main differences in the URODs from the three organisms are in the L1 and L2 loops (Fig. 3C). The presence of several positively charged residues, including the L1 loop, effect an obvious charge polarity on the electrostatic surface of the $UROD_{Bs}$ monomer (Fig. 3D).

There are a large number of proteins containing $(\beta/\alpha)_8$ barrel folds with different functions. For bacterial enzymes catalyzing nonoxidative decarboxylation, the $(\beta/\alpha)_8$ fold in a cofactor-free orotidine 5′-monophosphate decarboxylase was determined (1). However, this enzyme shows little structural similarity to $UROD_{Bs}$. Recently, a metal-dependent α-amino-β-carboxymuconic-ε-semialdehyde decarboxylase has also been identified as possessing the $(\beta/\alpha)_8$ fold (19, 23).

Active-site structure of $UROD_{Bs}$. The active-site structure in $UROD_{Bs}$ monomer A is similar to that in hUROD and tUROD. It is a deep cleft in a single domain surrounded by several flexible loops, including L1, L2, L3, L4, and L8, at the C-terminal end of the β-barrel. Aligning with the active-site structure of the hUROD-coprogen III complex, 18 amino acid residues in $UROD_{Bs}$, contacting at least one atom of the product ligand within 4.0 Å of the product, are displayed (Fig. 5A). They are Arg29 to Arg33, Ile74 to Asp78, Tyr38, Leu47, Phe144, Tyr154, Pro160, Phe207, Ser209, and H322. Among them, six residues are different from those in hUROD. The residues Tyr38, Leu47, Leu77, Tyr78, Lys79, and Pro160 in $UROD_{Bs}$ are replaced with Phe46, Phe55 Ile84, Phe85, Ser86, and Gly170, respectively, in hUROD. Ile92 and Pro98, equivalent to Met100 and Pro106 in hUROD, are not visible in the electron density map. In the active site, the residues are divided into three categories according to their function in substrate recognition and decarboxylation.

The first category contains Asp78 (Fig. 5A and B), which is involved in binding the pyrrole NH groups of the catalytic products and is precisely oriented by the formation of a hydrogen bond between its Oδ2 atom and the main-chain N atom of Met80. Two equivalent residues in hUROD are Asp86 and Leu88. The central coordination of the geometry of Asp86 allows substrates to be bound with equivalent activating interactions, which makes the partially decarboxylated intermediates bind and rebind in orientations of 90° about the contact point (28).

The second category includes a number of polar residues in the active cleft (Fig. 5B). An alignment of 39 sequences shows that four polar residues, Arg29, Arg33, Tyr154, and His322, are invariant (28). They may function in substrate binding and recognition through interactions with proporphyrinogen's side chains. Arg29 and Arg33 in $UROD_{Bs}$ are coordinated with carboxylate groups of the product, from the modeling of the hUROD-urogen III structure. Tyr154 seems not to be the key catalytic group in the decarboxylation reaction. An identical tyrosine in tUROD is proposed to protonate the α-position of the pyrrole ring in catalysis (21), but in hUROD, this role is not favored by site-directed mutagenesis studies and the determination of the complex structures (28). His322 is not crucial for decarboxylation, since the mutational analysis suggests that the analogous residue in hUROD is likely involved in the orientation of partially decarboxylated substrates (36).

The third category encompasses several hydrophobic amino acid residues (Fig. 5A and B). Their solvent-exposed hydrophobic side chains in the active-site cleft are proposed to be

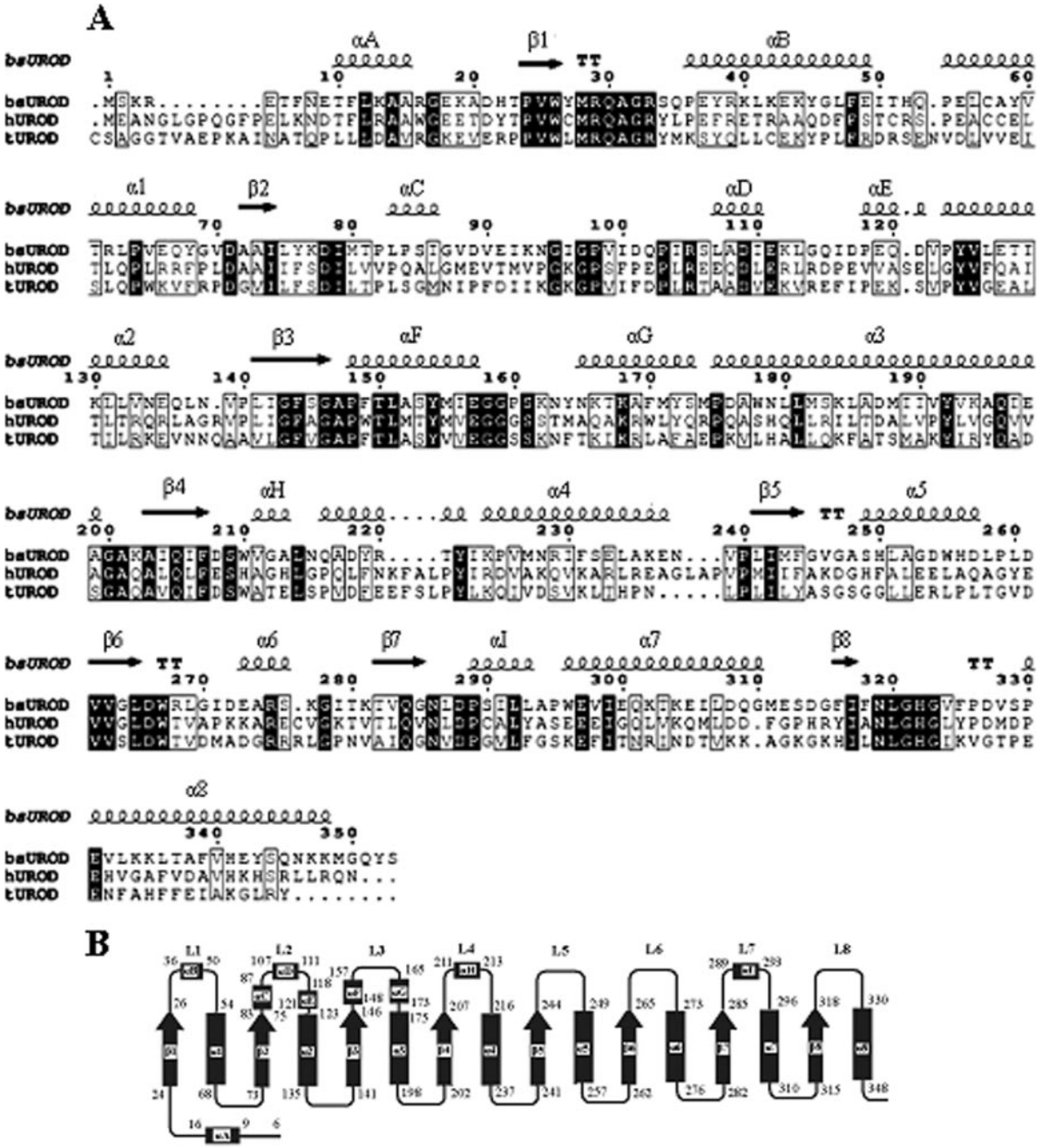

FIG. 4. (A) Structure-based sequence alignment of $UROD_{Bs}$ (bsUROD) with the human and tobacco enzymes. The secondary structure of $UROD_{Bs}$ is shown above its sequence. The image was produced using the program ESPript. Sequence alignment was performed using ClustalW. (B) Topological diagram of $UROD_{Bs}$ with the secondary structure elements indicated. Helices and strands are shown as bars and arrows, respectively. The first and last residues of each secondary structural element are numbered.

candidates for participation in substrate binding in a hydrophobic environment, contributing to catalysis by destabilization of the charged substrate with respect to the carbon dioxide product (28). Ala31 in $UROD_{Bs}$ is identical to Ala39 in hUROD that interacts with the C-ring propionate of the product via the apparent hydrogen bond in hUROD's complex structure, indicating that this carboxylate is protonated (28). Among the seven hydrophobic residues in $UROD_{Bs}$, Ile79, Phe144, and Phe207 are invariant (Fig. 5B).

Comparison of the secondary structure with those of hUROD and tUROD. There are some small differences in the lengths and positions of the secondary structural elements of bsUROD compared with those of tUROD and hUROD (Fig. 4A). In tUROD, the presence of Pro26 disrupts the first β sheet and thus forms the $(\beta\alpha)_7$ barrel fold, which has been found in several organisms by amino acid sequence alignments (21, 35). In $UROD_{Bs}$ and hUROD, a threonine is substituted at this position. Two helices, αE and α6, are

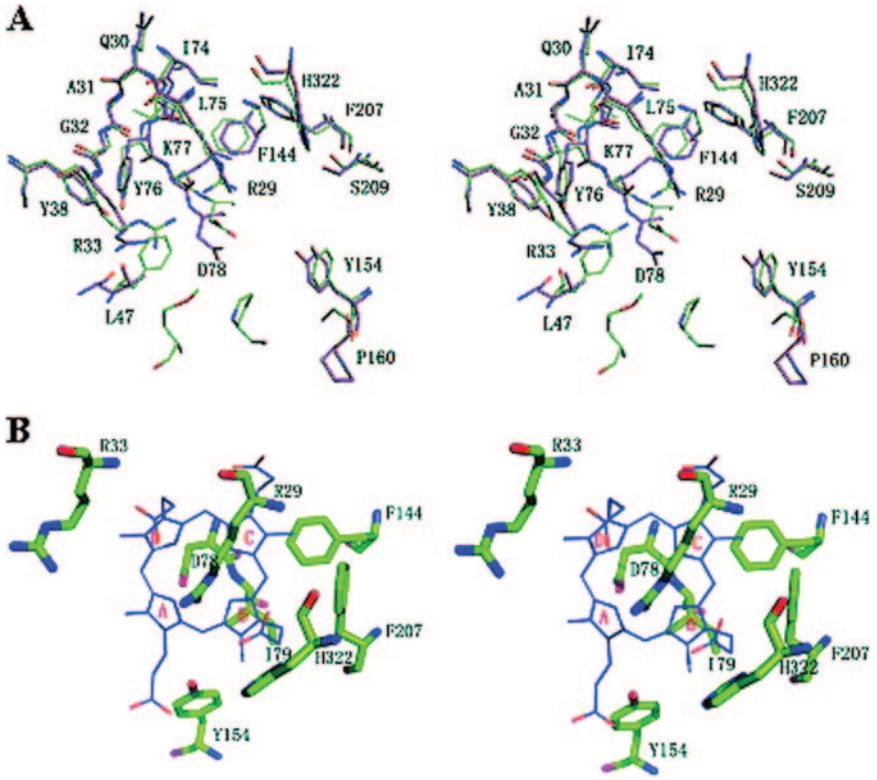

FIG. 5. A stereo view of the active sites from the $UROD_{Bs}$ monomer. (A) Eighteen amino acid residues within 4 Å of coprogen III are shown as sticks in $UROD_{Bs}$ (red) and in hUROD in complex with coprogen III (green). Ile79 is not labeled since it is not distinguished from other residues in the site. The residue numbering of $UROD_{Bs}$, from the first amino acid, methionine, is shown. (B) The invariant residues in the active site of $UROD_{Bs}$ modelled with coprogen III from the enzyme-product structure of hUROD.

one residue shorter in $UROD_{Bs}$ than in hUROD, and α4 is four residues shorter. On the contrary, α7 is one residue longer in $UROD_{Bs}$. The intervening loops between α2-β3 and α4-β5 in $UROD_{Bs}$ are one and three residues shorter, respectively. In hUROD, the identical L1 loop contains two short helices, and the identical L2 loop contains three short helices and two short β-sheets, whereas in $UROD_{Bs}$ a helix in the L1 loop and three helices in the L2 loop are displayed (Fig. 4B), suggesting that two loops as part of the active site are more flexible in $UROD_{Bs}$.

DISCUSSION

In this work, we report the first crystal structure of a bacterial UROD and its structural comparison with the human and tobacco homologues. However, based on the structures of URODs, the catalytic residues are not explained clearly and information about several special characteristics of UROD is not known. Therefore, we speculate on the possible functions of $UROD_{Bs}$ by extrapolation from the structural data.

Possible functional residues commonly existed in four designated enzymes. Since PBG and porphyrinogen, including urogen III and coprogen III, contain negatively charged carboxylate groups, the positively charged residues in the enzymes are essential for substrate recognition through hydrophilic interactions. In proteins, arginine residues are prime candidates. It was proposed that two arginine residues in *E. coli* UPMT (33), four arginine residues in human CPOX (18), and three arginine residues in human PBGD (17) might be involved in the binding of the respective substrates.

Anion coordination by the pyrrole nitrogen can create a cone conformation for the macrocycle (18). An aspartate interacting with a pyrrole NH group is proposed for *E. coli* PBGD and yeast and human CPOX (17, 18, 29). The central geometry of pyrrole's coordination by an aspartate, except in hUROD, is not identified in UPMT and CPOX, due mainly to the lack of the complex structures with a substrate or product. In the presence of an excess of UPMT, trimethyl and tetramethyl products are generated (31). The tetramethylation of urogen III at positions 2, 7, 12, and 18 is catalyzed by UPMT. At the same position on the side chains, decarboxylation is catalyzed by UROD. An aspartate in UPMT is proposed to interact with urogen III (33, 34). For two branch-point enzymes sharing common initial substrates, the urogen III binding site is a big trough in UPMT and a deep cleft in $UROD_{Bs}$, mainly due to the difference in the reactions catalyzed by the two respective enzymes.

It is thought that the catalytic mechanism of an aspartate in hUROD is analogous to that in PBGD (28). However, mutation of the equivalent aspartate in human PBGD to glycine results in the production of the first intermediate bound with the enzyme (17), suggesting that this residue may not play a key role in the initial reaction, and polymerization of PBG requires the aspartate to function in coordination with three

arginine residues. For *Pseudomonas denitrificans* UPMT, some residues, including Asp47 and Leu49, are proposed to contribute to the binding of urogen III. The Asp47Asn and Leu49Ala mutants generate the first methylated intermediate, precorrin-1 (34). As the exact urogen III binding site in UPMT is not determined, we envisage that the possible roles of two amino acid residues in UPMT are similar to the roles of Asp78 and Met80 in $UROD_{Bs}$. Leu49 in the UPMT may precisely orient Asp47, analogous to the role of Met80 in $UROD_{Bs}$.

Possible functions of two loops in $UROD_{Bs}$. The binding of substrates and release of products may be necessary for the coordinating function of the L1 and L2 loops in $UROD_{Bs}$. In the L1 loop, the small loop L1a includes Tyr27 to Asn36. Among them, four residues are invariant. Mutation of the invariant residue glycine in this small loop inactivates yeast UROD completely (9), possibly resulting from the change in this loop in which three amino acid residues associate with side chains of urogen III. The minor shift of two arginine residues is observed in the enzyme-product structures of hUROD liganded with coprogen III and isomer I (28). The symmetric nature of the urogen I structure suggests the active-site requirements of four decarboxylation reactions are essentially the same. Charge-charge interactions of the enzyme with urogen III may involve the attraction and binding of extra urogen III at high concentrations and induce the minor shift of L1a. Under these conditions, the restriction of the cleft on the asymmetric nature of the urogen III structure may be invalidated and a random sequence of decarboxylation occurs. In addition, the carboxylate groups of the substrate and the subsequent products might associate with the positively charged area and affect the binding of the substrate and release of the product.

The L2 loop comprises four small loops and three helices in $UROD_{Bs}$. The small loop L2a includes Asp78 and Met80. The absence of significant electron density for a dozen amino acid residues suggests real disorder in the small loop L2b in $UROD_{Bs}$. Comparison of $UROD_{Bs}$ with hUROD and tUROD shows that equivalent loops in the latter two structures also appear to have substantial flexibility, with high *B* values and broken electron density. The small loop L2b partially covers the opening to the active site. That the identical loop adopts the same conformation in the unliganded and product-bound structure of hUROD is thought to result in the binding of substrate and release of product with minimal change (28). Because the reaction proceeds through intermediate porphyrinogens with seven, six, and five carboxyl groups, the product-bound structures alone are not enough to provide information on the mobility of L2b. The minor shift of L2a, possibly caused by the mobility of L2b, affects the central coordination geometry of Asp78 in $UROD_{Bs}$. Observed alterations in the pattern of accumulation of intermediates might mainly reflect the mobility of L2b. For this reason, the first intermediate for UROD from *R. sphaeroides* is accumulated upon heating (16).

Amino acid residues possibly involved in catalysis. Based on the elucidation of the role of Asp86 in hUROD, we favor the idea that the preferred role of Asp78 in $UROD_{Bs}$ may be to participate in orienting urogen III for the sequential decarboxylation reactions. The protonated intermediate is promoted and generates Asp78, which delocalizes the positive charge on the pyrrole nitrogen. Because of the high π-electron density of the C_α atom of the pyrrole ring, the sequential decarboxylation route occurring via the sole residue Asp78 with the coordination of the pyrrole NH groups seems hardly credible. However, the exact location of the decarboxylation site is elusive with the available structural information. A complex structure of $UROD_{Bs}$ with the initial substrate would help to identify the catalytic residues. Unfortunately, attempts to obtain the cocrystal complex have been unsuccessful. The soaking experiments with 5 to 20 μM uroporphyrin III or isomer I also failed, since both oxidized substrates caused the destruction of the crystals.

More evidence, especially the failure to discover point mutations or chemical modifications that inactivate only one part of the decarboxylation process, suggests all decarboxylation happens at a unique site in the active cleft. According to the finding of sequentially clockwise decarboxylation, the first potential decarboxylation site may be occupied by the C ring pyrrole of the product. At this location, several hydrophobic residues orient the acetate side chain of the product, observed from the modeling of urogen III in the active site of $UROD_{Bs}$ (Fig. 5B). It is proposed that a ground-state destabilization of the energy of substrate binding may be dependent on the hydrophobic residues in hUROD (28), analogous to the mechanisms of other decarboxylases, including orotodine-5′-phosphate decarboxylase (1). However, the carboxylate binding sites of these decarboxylases contain hydrophobic and negatively charged residues. The cofactor-free nonoxidative orotodine-5′-phosphate decarboxylase contains an aspartate in close proximity to the carboxylate binding site, and the role of this residue has been disputed (1, 14). In $UROD_{Bs}$ and hUROD, no negatively charged residue is positioned in the carboxylate binding site (Fig. 5A). Obviously, the precise location of the substrate in $UROD_{Bs}$ is not the same as that of the product. Modification of URODs from rat livers and *R. sphaeroides* with the different arginine-selective reagents results in the complete inactivation of the enzyme (3, 16). Thus, Arg29 near the product's C-ring is recommended as a candidate for the binding of the acetate group of the substrate (Fig. 5B).

It is speculated that Arg29 in $UROD_{Bs}$ has dual roles. First, it could assist Asp78 in stabilizing a positive charge on a reaction intermediate. Second, it could position the acetate groups of the substrate to produce the scissile bond between the α- and β-positions. The decarboxylation of urogen III occurs through a tautomeric form of the pyrrole ring, as depicted for eukaryotic homologous enzymes (21, 28). When CO_2 is released from the substrate, the aromatic hydrogen of Phe144 and/or Phe207 might capture the CO_2 molecule. The proposed catalytic mechanism of $UROD_{Bs}$ is somewhat analogous to that of tUROD (21), but the functional residues in $UROD_{Bs}$ are different.

ACKNOWLEDGMENTS

Financial support to L.N. and M.T. for this project was provided by research grants from Chinese National Natural Science Foundation (grants 30121001, 30025012, and 30571066), the "973" plans of the Chinese Ministry of Science and Technology (grants 2004CB520801 and 2006CB806500), and the Chinese Academy of Sciences (grant KSCX1-YW-R-60).

REFERENCES

1. **Appleby, T. C., C. Kinsland, T. P. Begley, and S. E. Ealick.** 2000. The crystal structure and mechanism of orotidine 5′-monophosphate decarboxylase. Proc. Natl. Acad. Sci. USA **97:**2005–2010.
2. **Barnard, G. F., and M. Akhtar.** 1979. Stereochemical and mechanistic studies on the decarboxylation of uroporphyrinogen III in haem biosynthesis. J. Chem. Soc. Perkin Trans. I **13:**2354–2360.
3. **Billi de Catabbi S., M. C. Rios de Molina, and L. C. San Martin de Viale.** 1991. Studies on the active centre of rat liver porphyrinogen carboxylase in vivo effect of hexachlorobenzene. Int. J. Biochem. **23:**675–679.
4. **Brünger, A. T., P. D. Adams, G. M. Clore, W. L. Delano, P. Gros, R. W. G. Grosse-Kunstleve, J. S. Jiang, J. Kuszewski, M. Nilges, N. S. Pannus, R. J. Read, L. M. Rise, T. Simonson, and G. L. Warren.** 1998. Crystallography & NMR system: a new software suite for macromolecular structure determination. Acta Crystallogr. Sect. D. **54:**905–921.
5. **Collaborative Computational Project, Number 4.** 1994. The CCP4 Suite: programs for protein crystallography. Acta Crystallogr. Sect. D **50:**760–763.
6. **De Verneuil, H., S. Sassa, and A. Kappas.** 1983. Purification and properties of uroporphyrinogen decarboxylase from human erythrocytes. J. Biol. Chem. **258:**2454–2460.
7. **Elder, G. H., and A. G. Roberts.** 1995. Uroporphyrinogen decarboxylase. J. Bioenerg. Biomembr. **27:**207–213.
8. **Frankenberg, N., J. Moser, and D. Jahn.** 2003. Bacterial heme biosynthesis and its biotechnological application. Appl. Microbiol. Biotechnol. **63:**115–127.
9. **Garey, J. R., R. Labbe-Bios, A. Chelstowska, J. Rykta, L. Harrison, J. Kushner, and P. Labbe.** 1992. Uroporphyrinogen decarboxylase in *Saccharomyces cerevisiae.* HEM12 gene sequence and evidence for two conserved glycines essential for enzymatic activity. Eur. J. Biochem. **205:**1011–1016.
10. **Gouet, P., E. Courcelle, D. I. Stuart, and F. Metoz.** 1999. ESPript: analysis of multiple sequence alignments in PostScript. Bioinformatics **15:**305–308.
11. **Hansson, M., and L. Hederstedt.** 1992. Cloning and characterization of the *Bacillus subtilis hemEHY* gene cluster, which encodes protoheme IX biosynthetic enzymes. J. Bacteriol. **174:**8081–8093.
12. **Hansson, M., L. Rutberg, I. Schroder, and L. Hederstedt.** 1991. The *Bacillus subtilis hemAXCDBL* gene clusters, which encodes enzymes of the biosynthetic pathway from glutamate to uroporphyrinogen III. J. Bacteriol. **173:**2590–2599.
13. **Hippler, B., G. Homuth, T. Hoffmann, C. Hungerer, W. Schumann, and D. Jahn.** 1997. Characterization of *Bacillus subtilis hemN*. J. Bacteriol. **179:**7181–7185.
14. **Hur, S., and T. C. Bruice.** 2002. Molecular dynamic study of orotidine-5′-monophosphate decarboxylase in ground state and in intermediate state: a role of the 203–218 loop dynamics. Proc. Natl. Acad. Sci. USA **99:**9668–9673.
15. **Johansson, P., and L. Hederstedt.** 1999. Organization of genes for tetrapyrrole biosynthesis in gram-positive bacteria. Microbiology **145:**529–538.
16. **Jones, R. M., and P. M. Jordan.** 1993. Purification and properties of the uroporphyrinogen decarboxylase from *Rhodobacter sphaeroides*. Biochem. J. **244:**703–712.
17. **Jordan, P. M., A. Al-Dbass, L. A. McNeill, M. Sawar, and D. Butler.** 2003. Human porphobilinogen deaminase mutations in the investigation of the mechanism of dipyrromethane cofactor assembly and tetrapyrrole formation. Biochem. Soc. Trans. **31:**731–735.
18. **Lee, D. S., E. Flachsova, M. Bodnarova, B. Demeler, P. Martasek, and C. S. Raman.** 2005. Structural basis of hereditary coproporphyria. Proc. Natl. Acad. Sci. USA **102:**14232–14237.
19. **Li, T., H. Iwaki, R., Fu, Y. Hasegawa, H. Zhang, and A. Liu.** 2006. Alpha-amino-beta-carboxymuconic-epsilon-semialdehyde decarboxylase (AC-MSD) is a new member of the amidohydrolase superfamily. Biochemistry **45:**6628–6634.
20. **Luo, J., and C. K. Lim.** 1993. Order of uroporphyrinogen III decarboxylation on incubation of porphobilinogen and uroporphyrinogen III with erythrocyte uroporphyrinogen decarboxylase. Biochem. J. **289:**529–532.
21. **Martins, B. M., B. Grimm, H. P. Mock, R. Huber, and A. Messerschmidt.** 2001. Crystal structure and substrate binding modeling of the uroporphyrinogen-III decarboxylase from *Nicotiana tabacum.* Implications for the catalytic mechanism. J. Biol. Chem. **276:**44108–44116.
22. **Martins, B. M., B. Grimm, H. P. Mock, G. Richter, R. Huber, and A. Messerschmidt.** 2001. Tobacco uroporphyrinogen-III decarboxylase: characterization, crystallization and preliminary X-ray analysis. Acta Crystallogr. Sect. D **57:**1709–1711.
23. **Martynowski, D., Y. Eyobo, T. Li, K. Yang, A. Liu, and H. Zhang.** 2006. Crystal structure of alpha-amino-beta-carboxymuconate-epsilon-semialdehyde decarboxylase: insight into the active site and catalytic mechanism of a novel decarboxylation reaction. Biochemistry **45:**10412–10421.
24. **Moran-Jimenez, M. J., C. Ged, M. Romana, R. Enriquez De Salamanca, A. Taieb, G. Topi, L. D'Alessandro, and H. de Verneuil.** 1996. Uroporphyrinogen decarboxylase: complete human gene sequence and molecular study of three families with hepatoerythropoietic porphyria. Am. J. Hum. Genet. **58:**712–721.
25. **Murshudov, G. N., A. A. Vagin, and E. J. Dodson.** 1997. Refinement of macromolecular structures by the maximum-likelihood method. Acta Crystallogr. Sect. D **53:**240–255.
26. **Navaza, J.** 1994. AmoRe: an automated package for molecular replacement. Acta Crystallogr. Sect. A **50:**157–163.
27. **Phillips, J. D., F. G. Whitby, J. P. Kushner, and C. P. Hill.** 1997. Characterization and crystallization of human uroporphyrinogen decarboxylase. Protein Sci. **6:**1343–1346.
28. **Phillips, J. D., F. G. Whitby, J. P. Kushner, and C. P. Hill.** 2003. Structural basis for tetrapyrrole coordination by uroporphyrinogen decarboxylase. EMBO J. **226:**225–233.
29. **Phillips, J. D., F. G. Whitby, C. A. Warby, P. Labbe, C. Yang, J. W. Pflugrath, J. D. Ferrara, H. Robinson, J. P. Kushner, and C. P. Hill.** 2004. Crystal structure of the oxygen-dependent coproporphyrinogen oxidase (Hem13p) of *Saccharomyces cerevisiae*. J. Biol. Chem. **279:**38960–38968.
30. **Sasarman, A., P. Chartrand, R. Proschek, M. Desrochers, D. Tardif, and C. Lapointe.** 1975. Uroporphyrin-accumulating mutant of *Escherichia coli* K-12. J. Bacteriol. **124:**1205–1212.
31. **Sattler, I., C. A. Roessner, N. J. Stolowich, S. H. Hardin, L. W. Harris-Haller, N. T. Yokubaitis, Y. Murooka, Y. Hashimoto, and A. I. Scott.** 1995. Cloning, sequencing, and expression of the uroporphyrinogen III methyltransferase *cobA* gene of *Propionibacterium freudenreichii* (*shermanii*). J. Bacteriol. **177:**1564–1569.
32. **Straka, J. G., and J. P. Kushner.** 1983. Purification and characterization of bovine hepatic uroporphyrinogen decarboxylase. Biochemistry **22:**4664–4672.
33. **Stroupe, M. E., H. K. Leech, D. S. Daniels, M. J. Warren, and E. D. Getzoff.** 2003. CysG structure reveals tetrapyrrole-binding features and novel regulation of siroheme biosynthesis. Nat. Struct. Biol. **10:**1064–1073.
34. **Ve′vodova, J., R. M. Graham, E. Raux, H. L. Schubert, D. I. Roper, A. A. Brindley, A. I. Scott, C. A. Roessner, N. P. Starnford, M. E. Stroup, E. D. Getzoff, M. J. Warren, and K. S. Wilson.** 2004. Structure/function studies on a *S*-adenosyl-L-methionine-dependent uroporphyrinogen III C methyltransferase (SUMT), a key regulatory enzyme of tetrapyrrole biosynthesis. J. Mol. Biol. **344:**419–433.
35. **Whitby, F. G., J. D. Phillips, J. P. Kushner, and C. P. Hill.** 1998. Crystal structure of human uroporphyrinogen decarboxylase. EMBO J. **17:**2463–2471.
36. **Wyckoff, E. E., J. D. Phillips, A. M. Sowa, M. R. Franklin, and J. P. Kushner.** 1996. Mutational analysis of human uroporphyrinogen decarboxylase. Biochim. Biophys. Acta **1298:**294–304.
37. **Xu, K., V. Ndivo, and D. Majumdar.** 2002. Cloning and expression of *Chlorobium vibrioforme* uroporphyrinogen decarboxylase gene in a *Salmonella* heme auxotroph. Curr. Microbiol. **45:**456–458.